HSM2019-098

NUMERICAL AND EXPERIMENTAL ANALYSIS OF CHIP FORMATION AT ULTRAHIGH CUTTING SPEED

M. Storchak[1]*, H.-C. Möhring[1]

[1]University of Stuttgart, Institute for Machine Tools, Stuttgart, Germany

*Corresponding author; e-mail: michael.storchak@ifw.uni-stuttgart.de

Abstract

The tendency of substantially increasing the cutting speeds in the cutting processes of metallic materials leads to an increase in the productivity of the machining processes. In order to ensure such increase, the regularities of the cutting characteristics at the high cutting speeds should be examined more closely. For the analysis of chip formation at high cutting speed, cutting simulations were used together with experimental investigations of the orthogonal cutting process. Kinetic machining characteristics and characteristics of the chip morphology were investigated by experiment and analysed for cutting speeds from 1.17 to 25 m/s and different geometries of the cutting wedge. In addition, the characteristics were simulated with the help of the developed 2D FEM cutting model. The parameters of the constitutive equation for the FEM model were determined by experiment at correspondingly high cutting speeds. This ensured a good agreement between experimentally determined and simulated machining characteristics. In particular, chip formation was analysed for the critical cutting speeds at which the chip flow changes into a periodically serrated chip flow. When analysing the distribution of strain and temperature in the shear zones and the chip, it showed that these characteristics change depending on cutting speed for different tool orthogonal rake angles of the tool wedge.

Keywords:
Cutting; High-speed machining; Chip formation; Finite element simulation

1 INTRODUCTION

The machining of various metallic materials and alloys with ultrahigh cutting speed improves the machining process by decreasing the resistance of the work material and thus the energy required for machining [Arndt 1973]. A considerable increase in cutting speed leads to the embrittlement of the machined material, the decrease in its plastic strain during cutting and the transition from a continuous chip formation to the formation of segmental chips [Arndt 1975], [Sutter 1997], [Yousefi 2000]. These benefits from an increase in cutting speed have attracted the attention of various researchers. Hence, cutting with ultrahigh speed has been investigated since 1925 [Arndt 1973]. The effects resulting from that increase were examined by experiments, in analyses and simulations and published in various papers. Consequently, the main goal of cutting with ultrahigh speed was defined as an increase in material removal rate [Fernandez-Abia 2011].

Various publications are concerned with the analysis of cutting and chip forming processes at high cutting speed (see e.g. [Sutter 1997]). The chip morphology was analysed here with the adiabatic shear theory. It was found that adiabatic shear bands are formed in the case of segmental chips (see e.g. [Li 2017]). The effect of chip segmentation has a great influence on the surface quality of the machined workpiece and the tool life. In particular, this effect manifests itself in the cutting of steels and alloys that are hard to machine. Fernandez-Abia with colleges presented the analysis of the chip forming process as well as the kinetic machining characteristics and the surface quality in the machining of austenitic high-grade steels [Fernandez-Abia 2011]. Gu examined the chip forming process, especially the adiabatic shear evolution as well as the tool failure in the cutting of railway steels [Gu 2018]. Sutter and List analysed the chip forming process, the chip morphology and the forces during the machining of the popular titanium alloy Ti6AlV4 [Sutter 2013]. They suggested hypotheses on the chip formation of the titanium alloy at very high cutting speeds, based on the examination of the segmentation frequency. Sutter and Ranc carried out experiments of the temperature development in the chip during orthogonal high-speed cutting, thus forming a basis for the development of a simplified analytical temperature model [Sutter 2007]. Ye et. al. conducted extensive research into the critical cutting speed at which the transition from a continuous chip formation to the formation of segmental chips occurs, regarding different materials [Ye 2014]. With their investigations it is possible to predict this transition and thus to develop theoretical principles for the chip formation during machining processes with high cutting speeds.

In the last decades, examinations of high-speed machining have been aided by numerous numerical modellings and subsequent simulations. Based on the constitutive equation by e.g. Johnson-Cook, material models were worked out for the correspondingly high strain rates and plastic deformations in order to build numerical cutting models (see e.g. [Andrade 1994]). Marusich and Ortiz developed a

Lagrangian thermomechanical FE cutting model for the orthogonal high-speed cutting of heat-treatable steels [Marusich 1995]. The model was used for simulating chip formation, resultant forces and cutting temperatures. To simulate the machining process of hard-to-machine materials, Bäker [Bäker 2006], Hortig and Svedensen [Hortig 2007] as well as Owen and Vaz [Owen 1999] developed FE cutting models using material models adapted to high speeds. Zhang et. al. simulated the fracture behaviour of segmental chips numerically [Zhang 2016]. They analysed triaxiality stress, strain intensity and temperature development in the chip segmentation at high cutting speeds.

This paper presents experimental analyses and simulations of the cutting process and particularly of the chip morphology at high cutting speeds. It determines the range of the critical cutting speed at which the transition from a continuous chip formation to the formation of segmental chips occurs and compares it to kinetic characteristics of the machining process. These investigations can serve as a basis for the control of high-speed machining.

2 TEST SET-UP

Experimental tests were carried out during the orthogonal cutting of AISI 1045 heat-treatable steel on the machine tool Gildemeister CTX 420 linear. The mechanical and thermal properties of the material are given in Tab. 1.

The tool with a tightly clamped cemented carbide insert was fastened in a three-component dynamometer, type 9121 by Kistler. The dynamometer was put into a tool holder and made it possible to establish two components of the resultant force relevant for orthogonal machining processes, namely cutting force F_x and passive force F_z.

The signal by the piezo sensors of the dynamometer was converted into a voltage signal and amplified by means of an amplifier, type 5070 by Kistler. Then the signal was acquired with a measuring card, type Ni-6259 by National Instruments, and finally processed, analysed and visualized in the program environment LabVIEW.

Cemented carbide inserts, type SNMG-SM-1105 by Sandvik Coromant, were used. The experimental tests were conducted with three different tool orthogonal rake angles of the tool wedge of -10°, 0° and 10°. The angle of point is produced by grinding the flank face of the wedge at a corresponding tool orthogonal clearance, using a tool grinding machine. In all tests, the tool orthogonal clearance was constantly 8° and the depth of cut was 0.2 mm. The orthogonal cutting process was carried out at the following cutting speeds: 1.167 m/sec (70 m/min), 1.667 m/sec (100 m/min), 3.334 m/sec (200 m/min), 6.667 m/sec (400 m/min), 10 m/sec (600 m/min), 13.334 m/sec (800 m/min), 16.667 m/sec (1000 m/min), 20 m/sec (1200 m/min), 21.667 m/sec (1300 m/min), 25 m/sec (1500 m/min).

To examine the chip morphology, chips were collected after each cutting test and prepared as micrographs (see e.g. [Storchak 2016]). Lying on the end face, the individual chips were embedded in a silicone box filled up with a resinous compound. After the compound had finally hardened, samples were ground and polished. To analyse the microstructure, the polished sample surface was etched. Nitric acid with a concentration of 3% was chosen as etchant. An optical microscope Carl Zeiss Axio Observer was used to establish the chip geometry for determining the chip compression ratio and the distance between adjacent segments as well as to analyse the chip structure after etching.

Tab. 1: Mechanical and thermal properties of AISI 1045 steel [Material Data 2019].

Strength [MPa]		Elastic modulus [GPa]	Elongation [%]	Hardness [HB]	Poisson's ratio	Specific heat [J/kg•K]	Thermal expansion [µm/m•°C]	Thermal conductivity [W/m•K]
Tensile	Yield							
690	620	206	12	180	0.29	486	14	49.8

3 RESULTS OF EXPERIMENTS

The experimental part of the investigations into high-speed machining included the analysis of the kinetic cutting characteristics and the morphology of the chips produced in orthogonal cutting processes. The cutting process of AISI 1045 steel was examined for varying cutting speeds and tool orthogonal rake angles using full factorial design of experiments.

3.1 Kinetic machining characteristics

Fig. 1 shows the effect of cutting speed and tool orthogonal rake angel on cutting force. The average measurement uncertainty was for cutting force 8%.The cutting force decreased with growing tool orthogonal rake angle, which corresponded to the phenomenon well-known from literature (see e.g. [Heisel 2012]). With increasing cutting speed, there was a considerable decrease in cutting force, which was greatest in the range of minimal cutting speeds up to approx. 10 m/sec. The boundary depended on the size of the tool orthogonal rake angle. The lower or negative values of the tool orthogonal rake angle shifted this boundary towards lower cutting speeds (see Fig. 1).
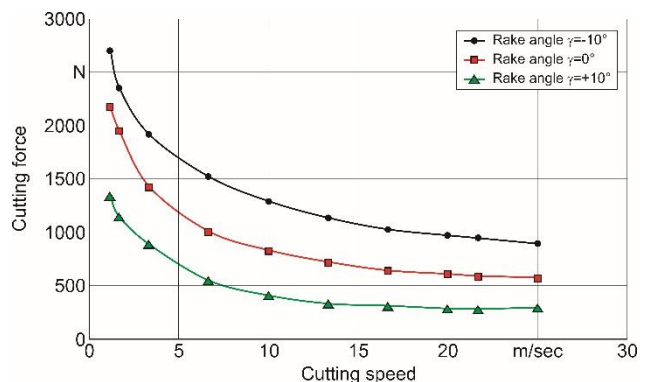
Fig. 1: Cutting force depending on cutting speed and tool orthogonal rake angle.

It is possible that this boundary corresponds to the critical cutting speed at which the transition from a continuous chip formation to the formation of segmental chips occurs (see [Ye 2014]). To examine the phenomenon more closely, the chip morphology was analysed at different cutting speeds (see Chapter 3.2).

The dependence of the thrust force on the tool orthogonal rake angle and the cutting speed maintains the character of the cutting force effect - Fig. 2. The average measurement uncertainty was for thrust force 12%. This concerns

especially the dependence on the tool orthogonal rake angle. The effect of the cutting speed was considerably less distinctive. Nonetheless, the substantial decrease in passive force showed in nearly the same range of cutting speed as in the case of the cutting force. This could suggest a characteristic change in the chip forming process, such as e.g. a transition from a continuous chip formation to the formation of segmental chips.
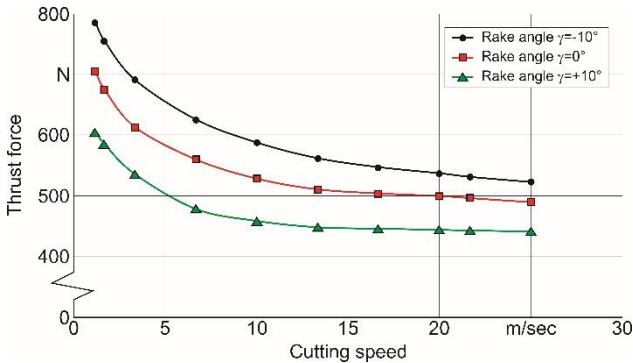
Fig. 2: Passive force depending on cutting speed and tool orthogonal rake angle.

Fig. **3** presents the chip compression ratio depending on tool orthogonal rake angle and cutting speed. The average measurement uncertainty was for chip compression ratio 10%. No definite effect of the tool orthogonal rake angle could be established from this dependence. However, the cutting speed showed a considerable effect on the chip compression ratio, similar to the effect on the resultant forces.
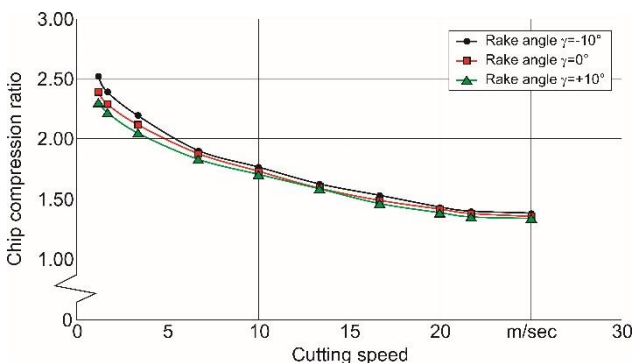
Fig. 3: Chip compression ratio depending on cutting speed and tool orthogonal rake angle.

It could be seen here that the absolute values of the chip compression ratio are considerably smaller for greater values of cutting speed than at conventional cutting speeds. This pointed to considerably smaller plastic deformations of the machined material at high cutting speeds and thus to lower energetic loads, even of the machining process.

3.2 Chip morphology

How often individual chip segments were formed could be assessed by analysing the distance between segments. Fig. **4** shows the distance between adjacent individual chip segments depending on tool orthogonal rake angle and cutting speed. The average measurement uncertainty was for segment distance of chip 14%. Analogously to the

dependences of kinetic machining characteristics, both the tool orthogonal rake angle and the cutting speed had a substantial effect on the segment distance. Like in the case of the resultant forces, the segment distance mainly decreased in the cutting speed range from 1.167 m/sec to approx. 10 m/sec. For greater values, the effect of the cutting speed was considerably smaller and the segment distance tended towards a constant value.
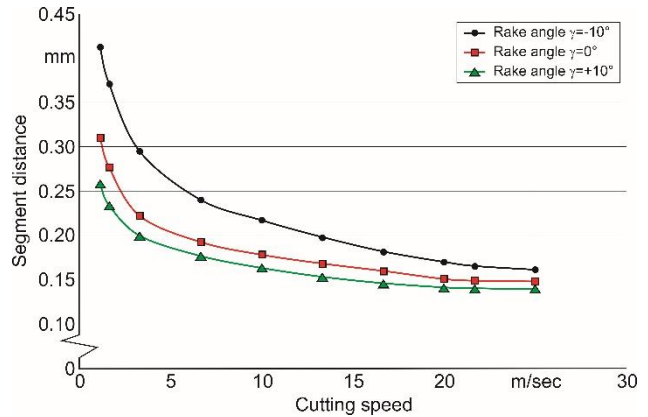
Fig. 4: Segment distance depending on cutting speed and tool orthogonal rake angle.

Tab. 2 presents the chip samples selected for the analysis of the microstructure at varying cutting speeds and tool orthogonal rake angles. In the analysis, it turned out that continuous chips were formed at a tool orthogonal rake angle of - 10° in the cutting speed range from 1.167 m/sec to 3.334 m/sec. The transition from the formation of continuous chips to segmental chips occurred in the cutting speed range between 3.334 m/sec and 6.667 m/sec. In order to exactly determine the critical cutting speed by experiment, additional tests with smaller incremental steps of the cutting speed will have to be carried out. It is also possible to develop an analytical/numerical model of the chip formation in high-speed machining for establishing the critical cutting speed. Regarding tool orthogonal rake angles of 0° and +10°, the transition from the formation of continuous chips to segmental chips occurred in the cutting speed range between 10 m/sec and 13.334 m/sec. Such a shift of the transition into higher cutting speeds could be explained by the smaller deformations of the machined material in the chip forming area when machining with greater tool orthogonal rake angles.

It depends on several factors where the critical cutting speed is. Primarily, the mechanical and thermal properties of the machined material, the physical-mechanical properties of its boundary layers, the geometry of the tool, the static and dynamic stiffness of the machine tool as well as several other factors have to be taken into account. Thus the exact determination of the critical cutting speed involves numerous experimental as well as analytical and numerical examinations, which will be carried out in future research.

Tab. 2 : Microstructure of chips.

Cutting speed [m/sec] ([m/min])	Rake angle [°]		
	-10	0	+10
1.167 (70)			
1.667 (100)			
3.334 (200)			
6.667(400)			
10.000 (600)			
13.334 (800)			
16.667 (1000)			
20.000 (1200)			
21.667 (1300)			
25.000 (1500)			
Metric scale	200 µm	200 µm	200 µm
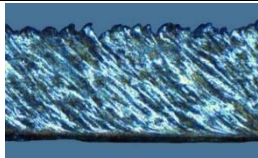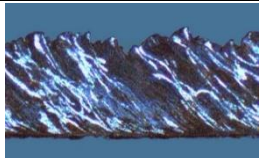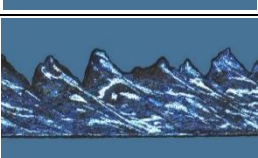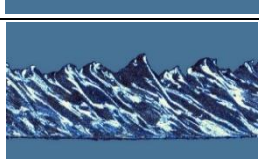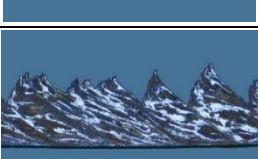
4 CUTTING SIMULATION

For the closer analysis of the phenomena accompanying machining processes at high cutting speeds, numerical simulations of the machining process were carried out in addition to the experimental tests. For that purpose, a 2D cutting model in the FEM software environment DEFORM 2D/3D™ v. 11.0 was worked out for simulating the machining of AISI 1045 steel. Fig. *5* presents the meshed geometrical model.
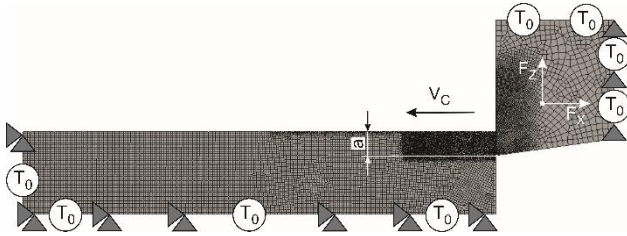
Fig. 5: Initial geometry and boundary conditions of orthogonal cutting model.

To improve the efficiency and the precision of the cutting model, the workpiece was meshed more finely in the shear zones as well as in the chip, and the tool was also meshed more finely in the contact areas with the workpiece and the chip. The mesh in the remaining areas was established more roughly. The boundary conditions were determined by fixing the workpiece and the tool as well as by the input of the thermal conditions at the boundaries of the respective objects. The bottom of the workpiece was rigidly fixed in the X- and Y-directions. The rigid fixation of the tool at the back of its rake face in Y-direction prevents its displacement in this direction. The thermal initial conditions at room temperature (RT) were given at the bottom and the left-hand side of the workpiece as well as at the right-hand side and the top of the tool. The working motion of the tool at a cutting speed V_C for guaranteeing the cutting process was given by the absolute motion in the negative X-direction.

The constitutive equation of Johnson-Cook was used to describe the material model [Johnson 1983]. The parameters of the constitutive equation were established by experiment according to the methodology worked out [Storchak 2019]. In order to reproduce the cutting process of AISI 1045 steel, the Cocroft and Latham model [Storchak 2016] was used as fracture model and the critical breaking stress was set to 200 MPa. Using a DOE (design of experiments) analysis, it was determined that the breaking stress and the load-carrying capacity of the finite elements were 10% after the fracture. The friction during the contact between the tool and the workpiece was modelled with a hybrid friction model. The model represented a combination of the Coulomb and the shear friction models. Regarding the modelling of the cutting process of AISI 1045 steel, the Coulomb friction coefficient was 0.15 and the plastic friction coefficient of the shear friction model was 0.6.

The functioning of the FEM cutting model was verified by simulating the chip formation, the development of the strain in the shear zones and in the chip as well as the temperature flows in the workpiece during machining. As an example, Fig. *6* illustrates the distribution of strain in the shear zones and the chip during the machining with a cutting speed of 10 m/sec and 20 m/sec as well as a tool orthogonal rake angle of the wedge of 0°.

Fig. *7* depicts the distribution of temperature in the shear zones (see also [Möhring 2018]) and the chip for the same cutting parameters and tool geometry.
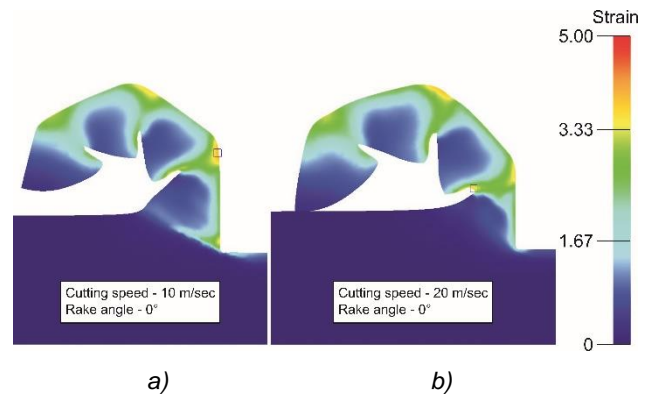
Fig. 6 : Distribution of strain in the chip and the shear zones (a - V$_C$=10 m/sec; b - V$_C$=20 m/sec).

The analysis of the simulation results, particularly the development of the chip formation, and their comparison with the experimental data (see

Tab. *2*) revealed that the created FEM cutting model was suitable for the further modelling.
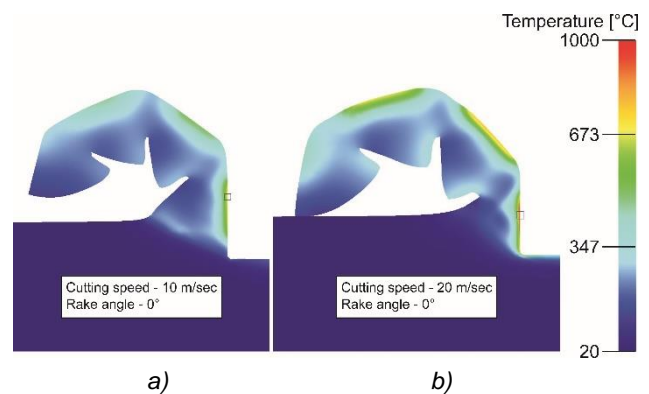
Fig. 7 : Distribution of temperature in the chip and the shear zones (a - V$_C$=10 m/sec; b - V$_C$=20 m/sec).

Further analyses were conducted regarding the development of strain and thermal flows in the workpiece as well as the effect of cutting speed and tool orthogonal rake angle on these two machining characteristics. The two machining characteristics were determined at the same point of the secondary shear zone, namely at the end of the plastic contact between the chip and the rake face of the wedge. Fig. *8* shows how the cutting speed affects the strain of the machined material for different tool orthogonal rake angles.
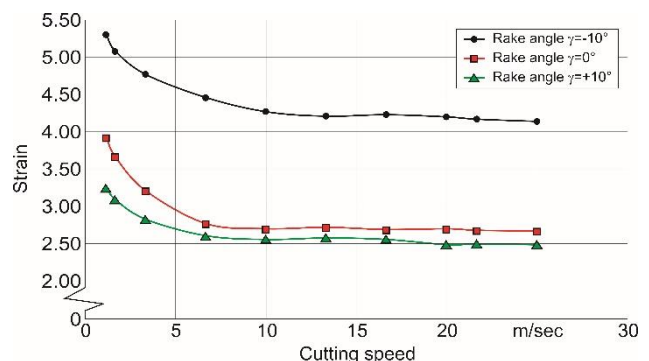
Fig. 8 : Effect of cutting speed on strain.

The strain decreased with growing cutting speed up to ca. 10 m/sec. When the cutting speed was increased further, the strain remained relatively constant and tended towards a particular value. This value was inversely proportional to the tool orthogonal rake angle. The decrease in strain with growing cutting speed helped the chip forming process and thus led to a reduction in the energy required for machining.

Fig. *9* depicts the dependence of maximum cutting temperature on cutting speed for different tool orthogonal rake angles. The cutting temperature increased considerably with growing cutting speed. The lower values of the tool orthogonal rake angle here guaranteed higher cutting temperatures. This led to the softening of the workpiece material and thus to a corresponding reduction in resultant forces. On the other hand, such an increase in cutting temperature resulted in a considerable increase in tool wear.
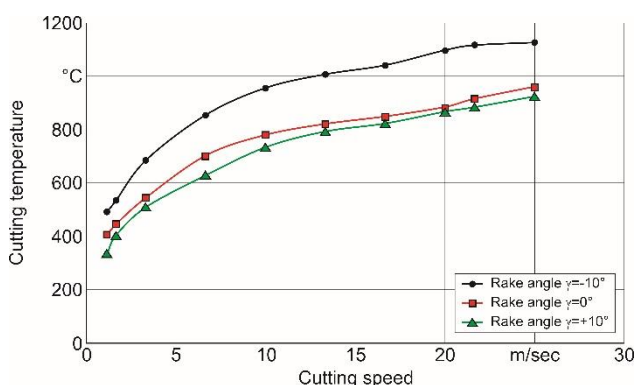
Fig. 9 : Cutting temperature depending on cutting speed.

The performed experiments as well as the created numerical cutting model and the simulations of orthogonal cutting processes formed the basis for developing productive and low-energy machining processes with high cutting speeds further.

5 SUMMARY

This study presents an analysis of the characteristics in orthogonal cutting of AISI 1045 steel at high cutting speeds in the range between 1.167 m/sec and 25 m/sec. The experimental tests and simulations of kinetic and thermal machining characteristics as well as of the chip morphology were aimed at forming a basis for controlling high-speed machining and developing productive as well as low-energy machining processes.

The experimental tests of the kinetic machining characteristics and the chip morphology showed a considerable dependence on the established values of the cutting speed and the tool orthogonal rake angle. The increase in cutting speed caused a considerable decrease in the resultant forces, the chip compression ratio and the distance between adjacent individual chip segments. The largest part of this decrease occurred in the range of small cutting speeds up to approx. 10 m/sec. The boundary depended on the size of the tool orthogonal rake angle. The smaller or negative tool orthogonal rake angles here shifted this boundary towards lower cutting speeds. By analysing the chip morphology, it was found out that this boundary corresponded to the critical cutting speed. The transition from a continuous chip formation to the formation of segmental chips occurred within the range of critical cutting speeds.

Using the developed FEM model of orthogonal cutting at high cutting speeds, it was analysed how the strain of the machined material and the temperature were distributed in the shear zones and the chip. This strain decreased with growing cutting speed up to approx. 10 m/sec. When the cutting speed was increased further, the strain remained relatively constant and tended towards a particular value. However, the cutting temperature increased considerably with growing cutting speed. The lower values of the tool orthogonal rake angle here guaranteed higher temperatures.

Consequently, high cutting speeds have an opposing effect. On the one hand, a further increase in cutting speed improves the machining process by decreasing the deformation energy required for machining. On the other hand, an increase in cutting speed leads to a greater wear of the tool due to the considerable increase in cutting temperature. Regarding an increase in cutting speed, there is surely a compromise or an optimum to be found separately for each individual machining process.

6 ACKNOWLEDGEMENTS

7 REFERENCES

[Arndt 1973] Arndt, G. Ultra-High-Speed Machining: A Review and an Analysis of Cutting Forces. Proceedings of the Institution of Mechanical Engineers, 1973, Vol.187, pp. 625-634.

[Arndt 1975] Arndt G. Ultra-High-Speed Machining: Notes on Metal Cutting at Speeds up to 7300 Ft/s. In: Tobias S. A., Koenigsberger F. (eds.) Proceedings of the Fifteenth International Machine Tool Design and Research Conference. Palgrave, London, pp. 203-208.

[Andrade 1994] Andrade, U. et. al. Dynamic Recrystallization in High-Strain, High-Strain-Rate Plastic Deformation of Copper. Acta Metallurgica et Materialia, 1994, Vol. 42, No. 9, pp. 3183-3195.

[Bäker 2006] Bäker, M. Finite element simulation of high-speed cutting forces. Journal of Materials Processing Technology, 2006, Vol. 176, pp. 117-126.

[Fernandez-Abia 2011] Fernandez-Abia, A. I. et. al. Effect of very high cutting speeds on shearing, cutting forces and roughness in dry turning of austenitic stainless steels. International Journal of Advanced Manufacturing Technology, 2011, Vol. 57, pp. 61-71.

[Gu 2018] Gu, L. The influences of adiabatic shear evolution on tool failure in high-speed machining of railway steel. Proceedings of the Institution of Mechanical Engineers, Part B: Journal of Engineering Manufacture, 2018, Vol. 232, Issue 6, pp. 1-6.

[Hortig 2007] Hortig, C., Svendsen, B. Simulation of chip formation during high-speed cutting. Journal of Materials Processing Technology, 2007, Vol. 186, pp. 66-76.

[Li 2017] Li, J. et. al. Study on the formation mechanism of saw-tooth chip in high-speed cutting process. Proceedings of the Institution of Mechanical Engineers, Part B: Journal of Engineering Manufacture, 2017, Vol. 231, Issue 14, pp. 2577-2584.

[Marusich 1995] Marusich, T. D., Ortiz, M. Modelling and Simulation of High-Speed Machining. International Journal for Numerical Methods in Engineering, 1995, Vol. 38, pp. 3675-3694.

[Owen 1999] Owen, D. R. J., Vaz Jr., M. Computational techniques applied to high-speed machining under adiabatic strain localization conditions. Computer Methods in Applied Mechanics and Engineering, 1999, Vol. 171, pp. 445-461.

[Sutter 1997] Sutter, G. et. al. Experimental Analysis of the Cutting Process and Chip Formation at High Speed Machining. Journal de Physique IV, 1997, Vol. 7, pp. 33-38.

[Sutter 2007] Sutter, G., Ranc, N. Temperature fields in a chip during high-speed orthogonal cutting - An experimental investigation. International Journal of Machine Tools & Manufacture, 2007, Vol. 47, pp. 1507-1517.

[Sutter 2013] Sutter, G., List, G. Very high speed cutting of Ti-6Al-4V titanium alloy – change in morphology and mechanism of chip formation. International Journal of Machine Tools & Manufacture, 2013, Vol. 13, pp. 37-43.

[Ye 2014] Ye, G. G. et. al. Critical cutting speed for onset of serrated chip flow in high speed machining. International Journal of Machine Tools & Manufacture, 2014, Vol. 86, pp. 18-33.

[Yousefi 2000] Yousefi, R., Ichida, Y. A study on ultra-high-speed cutting of aluminium alloy: Formation of welded metal on the secondary cutting edge of the tool and its effects on the quality of finished surface. Journal of the International Societies for Precision Engineering and Nanotechnology, 2000, Vol. 24, pp. 371-376.

[Zhang 2016] Zhang, X. et. al. Chip Fracture Behavior in the High Speed Machining of Titanium Alloys. Journal of Manufacturing Science and Engineering, 2016, Vol.138, Issue 8, pp. 081001-081001-14.

[Material Data 2019] Material Property Data. Available online: http://www.matweb.com (accessed on 19 April 2019).

[Heisel 2012] Heisel, U.; Kushner, V.; Storchak, M. Effect of machining conditions on specific tangential forces. Prod. Eng. Res. Dev. 2012, Vol. 6, pp. 621-629.

[Johnson 1983] Johnson G.R.; Cook W.H. A constitutive model and data for metals subjected to large strains, high strain and high temperatures. Proc. 7th Int. Symp. On Ballistics, The Hague, Netherlands, 1983, 541–547.

[Storchak 2019] Storchak, M.; Rupp, P.; Möhring, H.-C.; Stehle, T. Determination of Johnson–Cook Constitutive Parameters for Cutting Simulations. Metals 2019, Vol. 9, Issue 4, 473.

[Storchak 2016] Storchak, M.; Jiang, L.; Xu, Y.; Li, X. FEM Modelling for the Cutting Process of the Titanium Alloy Ti10V2Fe3Al. Prod. Eng. Res. Dev. 2016, Vol. 10, pp. 509-517.

[Möhring 2018] Möhring, H.-C.; Kushner, V.; Storchak, M.; Stehle, T. Temperature calculation in cutting zones. CIRP Ann. Manuf. Technol. 2018, Vol. 67, pp. 61–64.